Available online at www.sciencedirect.com
ScienceDirect
Journal of Power Sources 178 (2008) 163–173
JOURNAL OF POWER SOURCES
www.elsevier.com/locate/jpowsour

Development of high strength ferritic steel for interconnect application in SOFCs

J. Froitzheim [a], G.H. Meier [b], L. Niewolak [a], P.J. Ennis [a], H. Hattendorf [c], L. Singheiser [a], W.J. Quadakkers [a,*]

[a] *Forschungszentrum Jülich, Institute of Energy Research (IEF-2), D-52425 Jülich, Germany*
[b] *University of Pittsburgh, Department of Mechanical Engineering and Materials Science, 648 Benedum Hall, Pittsburgh, PA 15261, USA*
[c] *ThyssenKrupp VDM GmbH, R&D and Knowledge Management, Kleffstraße 23, 58762 Altena, Germany*

Received 30 July 2007; received in revised form 29 November 2007; accepted 8 December 2007

Abstract

High-Cr ferritic model steels containing various additions of the refractory elements Nb and/or W were studied with respect to oxidation behaviour (hot) tensile properties, creep behaviour and high-temperature electrical conductivity of the surface oxide scales. Whereas W additions of around 2 wt.% had hardly any effect on the oxidation rates at 800 and 900 °C, Nb additions of 1% led to a substantially enhanced growth rate of the protective surface oxide scale. It was found that this adverse effect can be alleviated by suitable Si additions. This is related to the incorporation of Si and Nb into Laves phase precipitates which also contribute to increased creep and hot tensile strength. The dispersion of Laves phase precipitates was greatly refined by combined additions of Nb and W. The high-temperature electrical conductivity of the surface oxide scales was similar to that of the Nb/W-free alloys. Thus the combined additions of Nb, W and Si resulted in an alloy with oxidation resistance, ASR contribution and thermal expansion comparable to the commercial alloy Crofer 22 APU, but with creep strength far greater than that of Crofer 22 APU.

Keywords: SOFC; Interconnect; Ferritic steel; Creep; Oxidation; Conductivity

1. Introduction

High-Cr ferritic steels are under consideration as construction materials for interconnects in planar solid oxide fuel cells (SOFCs) [1–9]. Fundamental studies, as well as more technologically orientated research, have been conducted using commercially available materials and steels especially designed for SOFC application [2–5]. The latter materials were optimised mainly with respect to thermal expansion coefficient, electrical conductivity of the surface oxide scales, reduced Cr evaporation and/or improved workability. A major drawback of ferritic steels is their poor creep resistance at the high SOFC operating temperatures in the range 700–900 °C. Steels especially designed for interconnect applications even tend to show reduced creep resistance because the mentioned optimisation of SOFC relevant properties frequently could only be achieved by reducing the concentrations of minor alloying additions (such as Si and Al) and impurities, which are commonly present in steels [3]. The poor creep resistance may not be a critical issue in some stack designs, but especially for designs in which interconnects with a thickness of only a few tenths of a millimetre are being envisaged [10], creep resistance of the interconnect material is expected to be of great importance for long-term stack operation.

This paper presents the results of an investigation aimed at the development of ferritic steels with enhanced creep resistance without substantially degrading the other important SOFC relevant properties mentioned above. For this purpose a number of ferritic model alloys were subjected to isothermal oxidation tests using thermogravimetric analyses (TGA) at temperatures in the range 700–1000 °C, long-term oxidation tests in air (800 and 900 °C), creep tests (700 and 800 °C), and tensile tests in the temperature range between room temperature and 800 °C as well as in situ studies of the electrical conductivity of the surface oxide scales at 800 °C.

* Corresponding author. Tel.: +49 2461 61 4668; fax: +49 2461 61 3687.
E-mail address: j.quadakkers@fz-juelich.de (W.J. Quadakkers).

0378-7753/$ – see front matter © 2007 Elsevier B.V. All rights reserved.
doi:10.1016/j.jpowsour.2007.12.028

Table 1
Chemical composition of investigated steels measured by ICP-OES

Alloy	Cr (Wt.%)	Mn (Wt.%)	La (Wt.%)	Ti (Wt.%)	Nb (Wt.%)	W (Wt.%)	Al (Wt.%)	Si (Wt.%)	C (ppm)	S (ppm)	N (ppm)	O (ppm)
Reference	23.2	0.53	0.16	0.06	–	–	<0.01	0.03	40	30	100	50
1% W	22.3	0.51	0.12	0.09	–	0.9	0.01	0.05	40	30	40	70
2.7% W	20.6	0.53	0.13	0.11	–	2.7	0.01	0.06	20	20	60	50
1% Nb	22.2	0.52	0.16	0.15	1.1	–	0.01	0.02	100	30	170	60
1% Nb + 0.25% Si	22.2	0.50	0.12	0.1	1.0	–	0.01	0.25	30	20	170	70
1% Nb + 0.42% Si	22.5	0.43	0.09	0.06	1.0	–	<0.01	0.42	20	<20	160	70
2% W + 0.5% Nb + 0.25% Si	22.3	0.43	0.06	0.06	0.5	2.0	<0.01	0.24	<20	<20	70	80

2. Experimental

2.1. Manufacturing of the alloys

The composition of the previously described ferritic high-Cr steel JS-3 [1,3] was used as the basis for the variation in composition of the model alloys (Table 1). A commercially available steel with the same chemical composition as JS-3 is designated Crofer 22 APU [2]. For obtaining increased creep strength of the steel, two mechanisms may be used: precipitation strengthening and/or solid solution strengthening. Nb is well known to form Laves phase precipitates of the type Fe_2Nb at small additions of Nb. Due to its large atomic radius and high solubility in α-Fe, W is an element which is potentially suitable to impart substantial solid solution strengthening. Therefore W and Nb were added in various amounts (0.5–2 wt.%) to the base alloy composition of JS-3. The effect of the common minor alloying additions, e.g. Si in concentrations of a few tenths of a percent, was included in even the studies. Some of the elements, particularly Si and Ti, are known to oxidise internally during high-temperature exposure. Depending on the extent and morphology of internal oxidation connected with this sub-scale formation, the growth rate of the external duplex surface scale, consisting of Cr-oxide and Cr/Mn-spinel can be adversely affected [1–3,9,11–15].

The alloys were manufactured by ThyssenKrupp VDM by vacuum melting and ingots of approximately 10 kg were cast and subsequently hot rolled to plates of 2 and 16 mm thickness. Specimens of dimensions 20 mm × 10 mm × 2 mm or 10 mm × 10 mm × 2 mm were machined for oxidation and conductivity testing from the 2-mm thick plates. The 16-mm thick plates were used for manufacturing standard specimens for tensile and creep tests.

2.2. Oxidation behaviour

Discontinuous oxidation tests were carried out at 800 and 900 °C in laboratory air, whereby the specimens were cooled to room temperature every 250 h for weight measurements. The isothermal oxidation experiments were carried out in synthetic air (mixture of nitrogen with 20 vol.% oxygen) using a microbalance (Setaram TG 92). The specimens were heated to the test temperature with a rate of 90 K min^{-1}, kept at temperature for 72 h, and subsequently furnace cooled. The oxide scales formed during the oxidation tests were studied by scanning electron microscopy (SEM) with energy dispersive X-ray analysis (EDX)

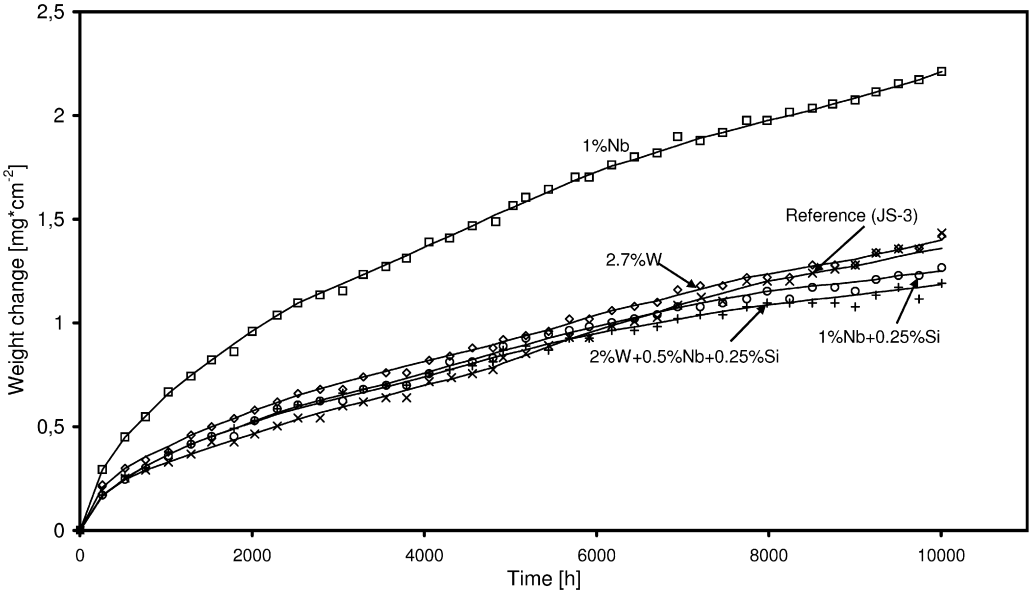

Fig. 1. Weight change as a function of time during discontinuous oxidation of model steels at 800 °C in air.

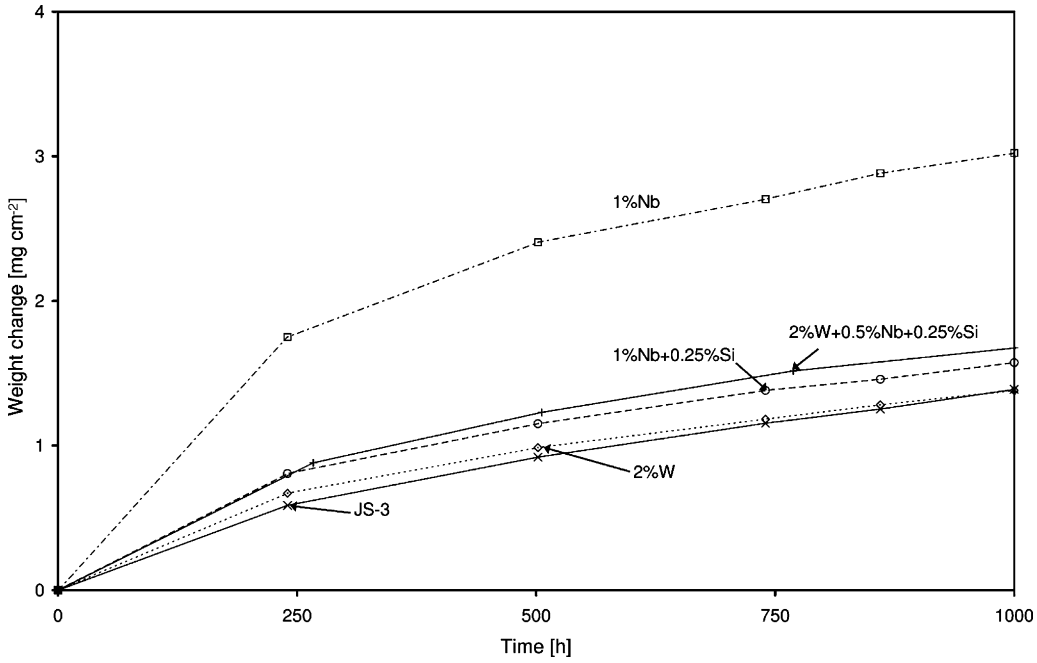

Fig. 2. Weight change as a function of time during discontinuous oxidation of model steels at 900 °C in air.

or wavelength dispersive X-ray analysis (WDX). Additionally, for detailed investigation of oxide scale microstructures, the FIB/TEM (focused ion beam/transmission electron microscopy) technique was used.

2.3. Contact resistance measurements

The contact resistances of the oxide scales were measured using a conventional four-point method. Specimens of 10 mm × 10 mm × 2 mm were ground to a 1200 grit surface finish and then pre-oxidised for 100 h at 800 °C in air. Subsequently, a layer of Pt-paste was applied to both oxidised surfaces and a Pt-mesh was used for electrical connection. The contact resistance was monitored in situ for 300 h of exposure at 800 °C in air and subsequently during step-wise cooling to 750, 700, 650, and 600 °C, each temperature stage was run for 10 h. The exposure times were limited to 300 h because it was previously shown that during longer exposure times the oxidation kinetics and the oxide scale morphology became substantially affected by the presence of a deposited Pt-contact layer [16]. At least two specimens were tested for each material to check the reproducibility of the results.

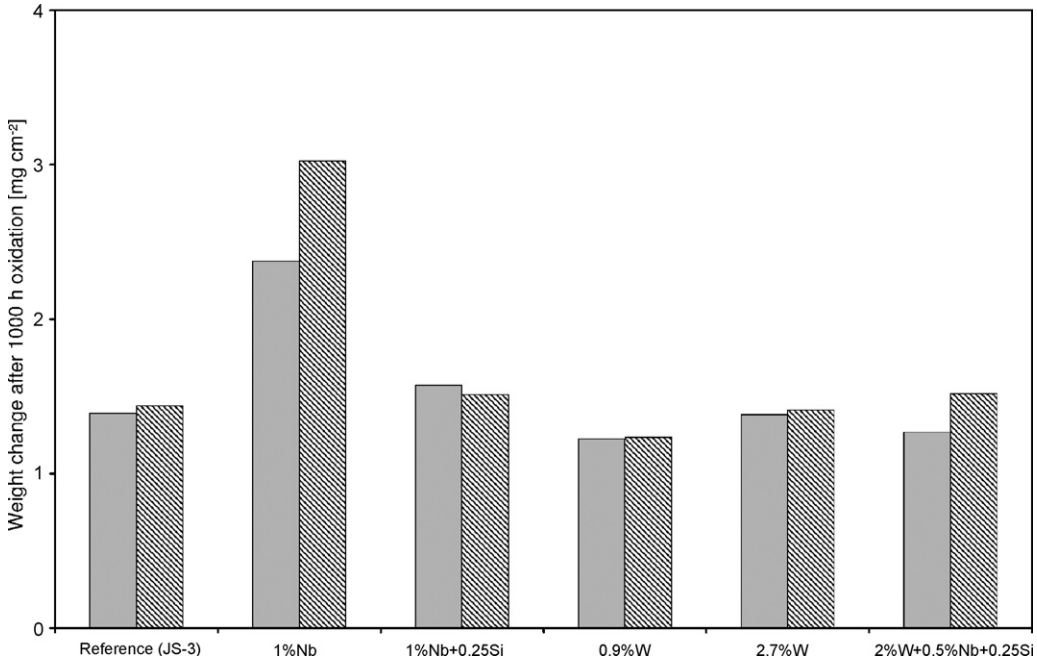

Fig. 3. Weight change after 1000 h discontinuous oxidation of model steels with various alloying additions at 900 °C in air (duplicate specimens).

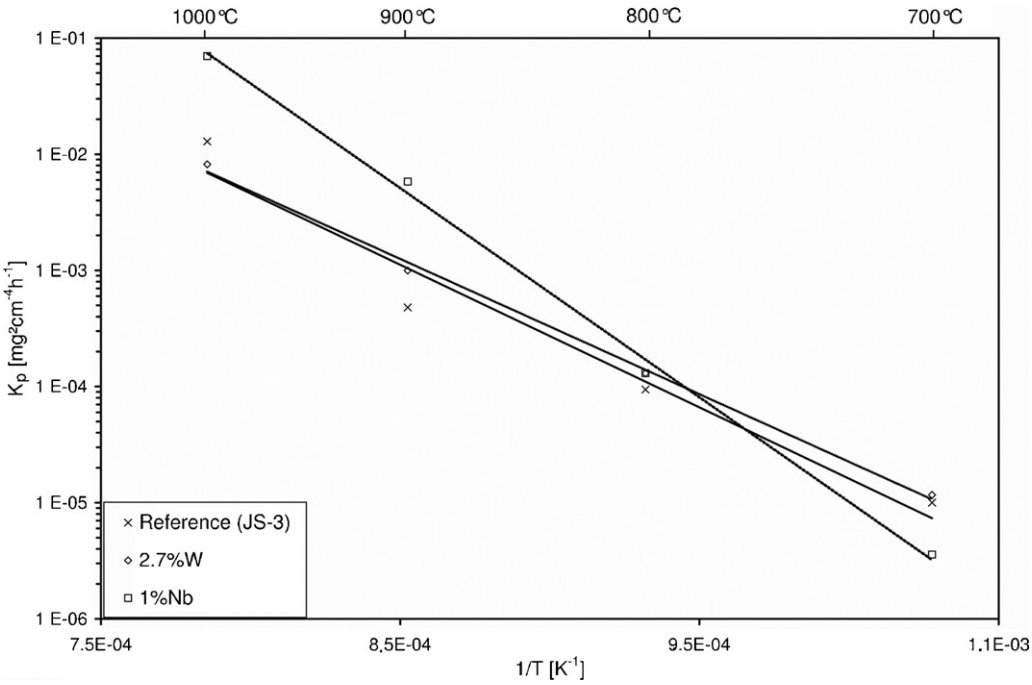

Fig. 4. Parabolic rate constant K_p as a function of reciprocal temperature for selected steels during isothermal oxidation for 72 h in air.

2.4. Creep tests

For the creep tests, cylindrical specimens were machined from the 16-mm thick plates. The specimens were 6.4 mm in gauge diameter and the gauge length was 50 mm. Creep tests were performed at 700 and 800 °C in air at a constant stress of 10 MPa, whereby the specimens were cooled to room temperature after the first 500 h and later every 1000 h for strain measurements.

3. Results and discussion

3.1. Oxidation tests

Figs. 1 and 2 show weight change data for the investigated steels during discontinuous oxidation at 800 and 900 °C in laboratory air. The alloy with 1% Nb addition showed the highest oxidation rate of the tested alloys at both temperatures. Steels alloyed with 2.7% W or 1% Nb + 0.25% Si or 2% W + 0.5%

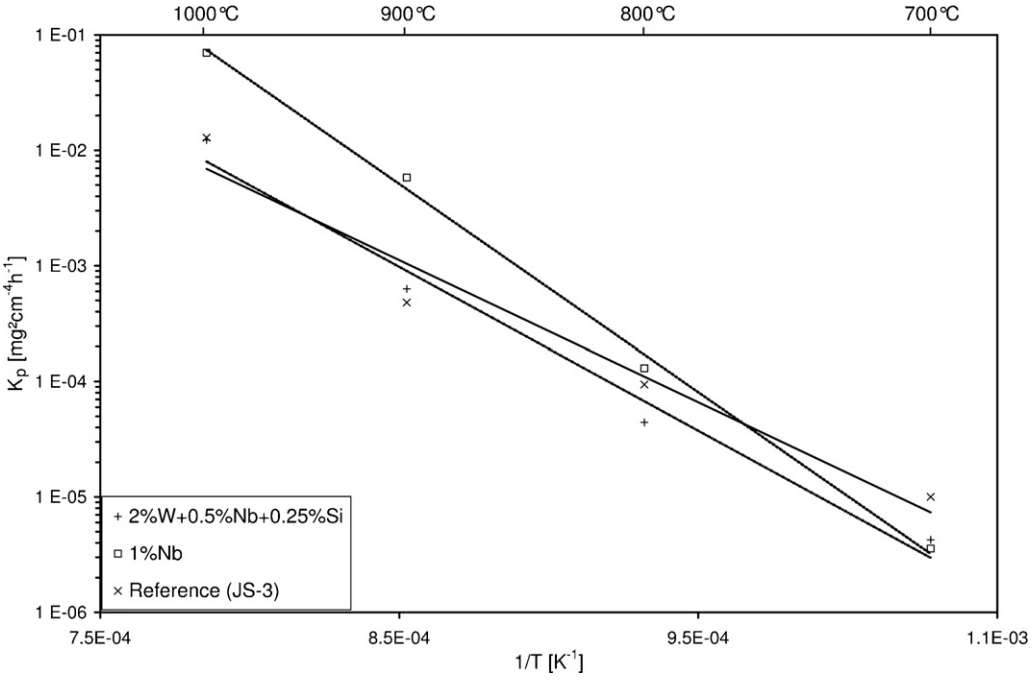

Fig. 5. Parabolic rate constant K_p as a function of reciprocal temperature for selected steels during isothermal oxidation for 72 h in air.

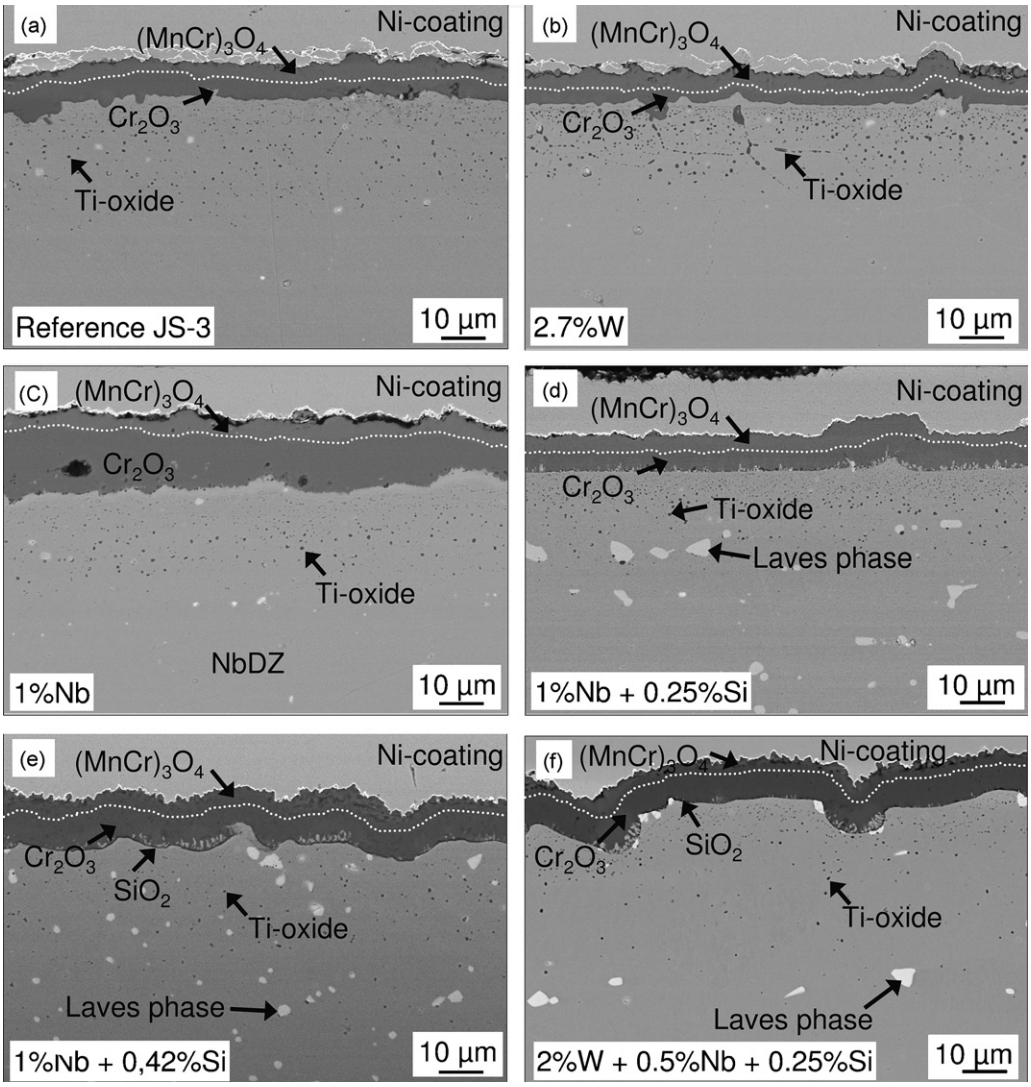

Fig. 6. SEM/BSE images showing cross-sections of steel specimens oxidised for 1000 h at 900 °C in air: (a) JS-3, (b) 2.7% W, (c) 1% Nb, (d) 1% Nb + 0.25% Si, (e) 1% Nb + 0.42% Si, and (f) 2% W + 0.5% Nb + 0.25% Si. The 1% Nb alloy exhibits a wide Nb-depleted zone (NbDZ) so that the Laves phase precipitates cannot be seen in (c).

Nb + 0.25% Si exhibited oxidation rates which were similar to that for JS-3. The weight gains after 1000 h oxidation at 900 °C in air are compared in a bar chart in Fig. 3. No spallation was observed when the specimens were cooled to room temperature for the weight change measurements. The 1000 h weight changes were seen to be quite reproducible for the duplicate specimens except in the case of the 1% Nb alloy which showed the most rapid scale growth. The 72 h isothermal oxidation data (TGA) were used to calculate parabolic rate constants presented as Arrhenius plots in Figs. 4 and 5. It is observed that the rate constant for 2% W + 0.5% Nb + 0.25% Si is somewhat smaller than that of JS-3.

Fig. 6 shows the differences in oxide scale morphologies and alloy microstructures of the studied materials after 1000 h discontinuous oxidation at 900 °C in air. In all cases the oxide scale consisted of an outer $(Mn,Cr)_3O_4$ layer and an inner Cr_2O_3 layer. An internal oxidation zone of Ti oxides also formed in each alloy. The particular oxide of Ti was not identified but, based on the thermodynamic properties of the Ti–O system and results for similar alloys with higher Ti concentrations [17], it is presumed to be Ti_2O_3 and/or Ti_3O_5. The depth of the internal oxidation zone varied for the studied alloys from approximately 30 μm for JS-3 to approximately 10 μm for the alloy with 2% W + 0.5% Nb + 0.25% Si addition. No evidence for the formation of internal silica precipitation in the internal oxidation zone was found. The most apparent differences in the scale morphologies on the studied steels were an increased oxide scale thickness and the presence of an Nb-rich oxide layer near the alloy/scale interface in the case of the steel with a 1% Nb addition (Fig. 6c). The scale on the alloy with additions of 1% Nb and 0.25% Si exhibited the most uniform oxide scale (Fig. 6d).

Fig. 7 presents electron micrographs of FIB cross-sections of three of the alloys. TEM/EDX analysis showed that the chemical composition of the Nb-rich layer in the alloy with 1% Nb is close to 41% Nb, 10% Cr, 3% Ti and 46% O (in at.%). The growth of this layer led to formation of an Nb-depleted zone (NbDZ) in

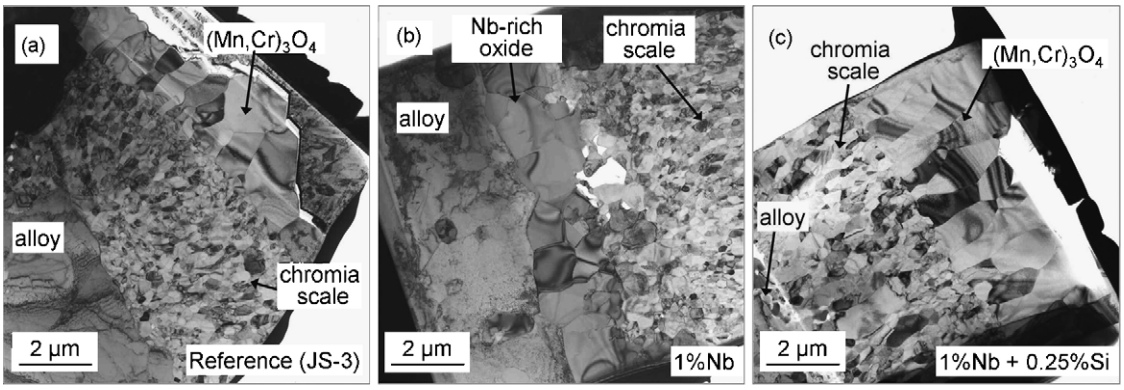

Fig. 7. TEM images showing microstructures of the oxide scales formed during 1000 h discontinuous oxidation at 900 °C in air: (a) JS-3, (b) 1% Nb, and (c) 1% Nb + 0.25% Si.

the alloy (Fig. 6b). This zone reached ca. 100 μm after 1000 h oxidation at 900 °C in air. The increased growth rate of the oxide scale formed on the 1% Nb-containing steel seems to be related to an enhanced growth of the chromia layer and to formation of the Nb-rich oxide at the metal/scale interface. It is postulated that Nb can dope Cr_2O_3 as Nb^{2+}, Nb^{4+} and Nb^{5+} depending on the position in the oxide scale, i.e. the persisting oxygen activity. Based on literature data which considered the influence of doping elements, e.g. Ti ions on the growth rate of chromia scales, it is believed that doping of Cr_2O_3 by Nb^{4+} or Nb^{5+} can increase its growth rate in a similar manner as Ti [18,19].

Studies on the oxidation behaviour of the model steels in simulated anode gas revealed a similar gas composition dependence of the oxidation behaviour as previously found for JS-3 and other materials with double-layered scales consisting of Cr_2O_3 and $MnCr_2O_4$. The oxidation rates in simulated anode gas were slightly smaller than those found in air [16,20]. The outer spinel layer exhibits a morphology of facetted crystals after air exposure and a blade and whisker like morphology after anode gas exposure. A more extensive description of the results in various simulated anode gases falls outside the scope of this paper and will be presented in a separate publication.

3.2. Microstructural investigation

JS-3 possesses a single-phase α-Fe(Cr) microstructure. The addition of 0.5 wt.% or more of niobium resulted in the formation of a two-phase microstructure (Fig. 6d–f) consisting of large ferrite grains and precipitates of Laves phase $(Fe,Cr)_2Nb$ [21–24]. Laves phase strengthening of ferritic/martensitic steels especially for applications in the range 600–650 °C has been extensively described in Refs. [21,22]. Silicon at a level of 0.25 wt.% appeared to be nearly completely dissolved in the Laves phase. In agreement with the binary Fe–Nb and ternary Fe–Cr–Nb phase diagrams, XRD and electron diffraction confirmed Laves phase precipitates embedded in an α-Fe matrix. According to SEM/EDX analyses the Laves phase precipitates present in the alloy with 1% Nb and 0.25% Si had the composition Fe–40% Nb–9.5% Cr–2.5% Si (in wt.%) (see Table 2). Silicon dissolved in the $(Fe,Cr)_2Nb$ phase appeared to suppress the formation of the Nb-rich oxide layer and the Nb-depleted zone (NbDZ) caused by oxidation of niobium (compare Fig. 6c and d). This is the result of a strong interaction between the Nb and Si which is discussed below. Additions of up to 2.7 wt.% of tungsten were dissolved completely in the α-Fe(Cr) matrix and did not significantly change the phase composition and microstructure of the steel (Fig. 6b). Combined additions of 2% W with 0.5% Nb and 0.25% Si resulted in the formation of a two-phase microstructure with more evenly distributed finer precipitates of Laves phase. This is illustrated in Fig. 8 where the Laves phase distribution for the 1% Nb + 0.25% Si and 2% W + 0.5% Nb + 0.25% Si alloys are compared after 1000 h exposure in air at 800 °C. SEM/EDX analyses of the α-Fe(Cr,W) and Laves phase precipitates present in the alloy revealed that

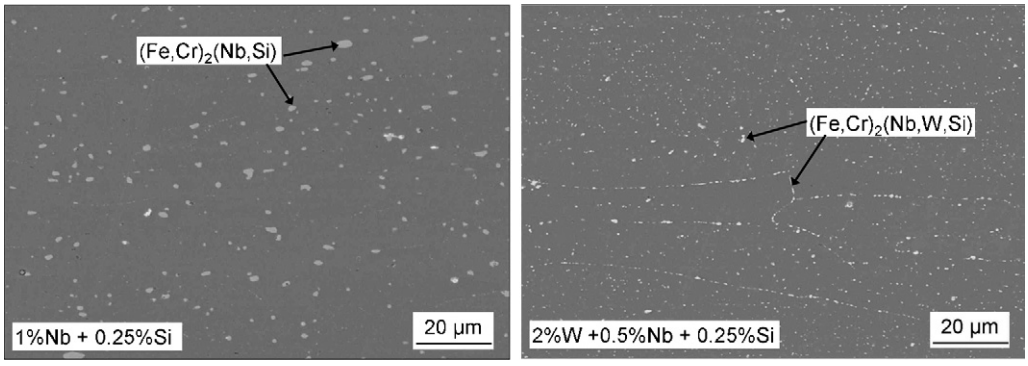

Fig. 8. Microstructures of Laves phase strengthened steels after 1000 h exposure at 800 °C in air.

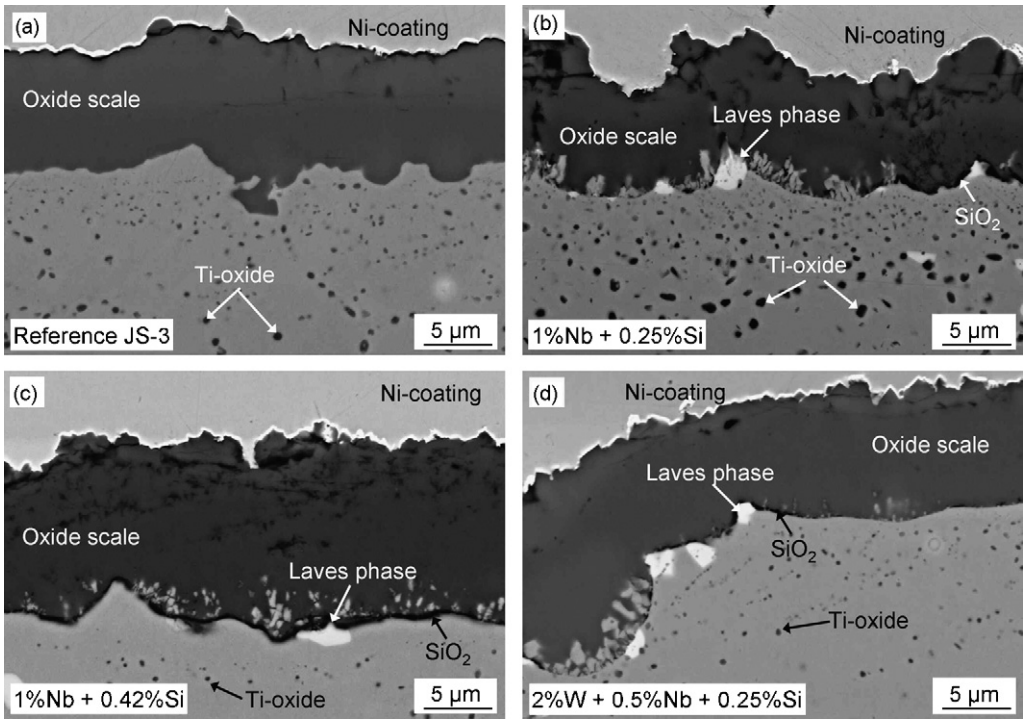

Fig. 9. SEM/BSE images showing cross-sections of oxide scales formed during 1000 h oxidation at 900 °C in air: (a) JS-3, (b) 1% Nb, (c) 1% Nb + 0.42% Si, and (d) 2% W + 0.5% Nb + 0.25% Si.

Table 2
Chemical composition of the phases in selected alloys

Element	Chemical composition (wt.%)			
	1% Nb + 0.25% Si (EDX)		2% W + 0.5% Nb + 0.25% Si (WDX)	
	Alloy matrix	Laves phase	Alloy matrix	Laves phase
Fe	77	48	76.5	43.5
Cr	23	9.5	21	8
Nb	0[a]	40	0.2[a]	25
W	–	–	1.5	21.5
Si	0[a]	2.5	0.2[a]	1.5

[a] Values near or below detection limits of the used method.

approximately 50% of the added tungsten is dissolved in the Laves phase.

Normally the additions of Si at the levels studied here would result in formation of internal silica precipitates and sometimes, even a near continuous layer of silica at the chromia/alloy interface [25]. Mikkelsen et al. [26] found that an addition of 0.15 wt.% Si to an Fe–21%Cr alloy resulted in the formation of vitreous silica precipitates which covered a significant fraction of the chromia/alloy interface after 24 h oxidation at 900 °C. However, the presence of the Nb additions has reduced this tendency.

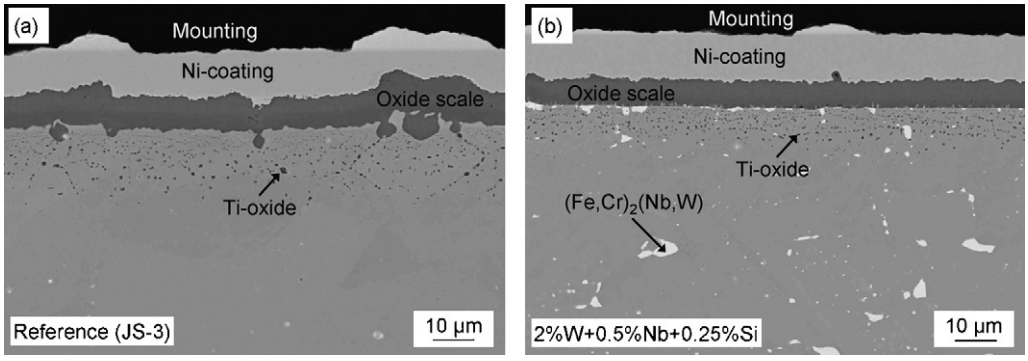

Fig. 10. SEM/BSE images showing cross-sections of oxide scales formed during 10,000 h oxidation at 800 °C in air: (a) JS-3 and (b) 2% W + 0.5% Nb + 0.25% Si.

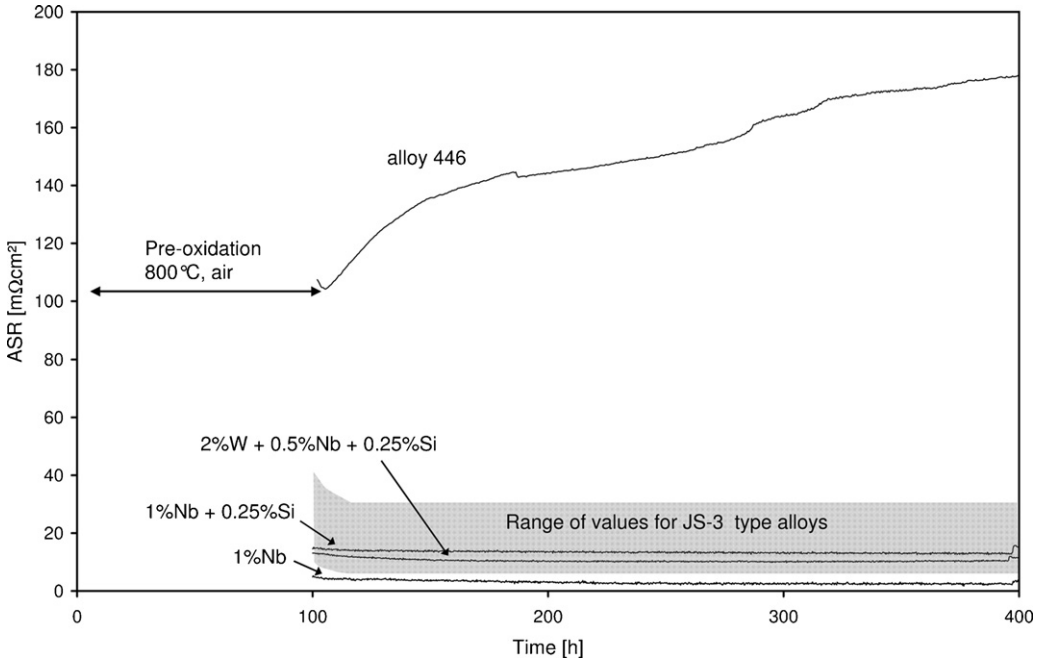

Fig. 11. ASR as a function of time for investigated steels measured at 800 °C in air. The ASR range for JS-3 type alloy was achieved by measurements on 18 specimens. Data for alloy 446 (ferritic steel with 24% Cr, 0.4% Si, no Nb) were taken from Ref. [27].

The combined additions of Nb and Si simultaneously reduced the tendency for Nb oxides to be present in the scale, which occurs for Nb additions alone, and for the formation of silica films at the chromia/alloy interface, which would occur for Si additions alone. There are limited thermodynamic data available for the Fe–Cr–Nb–Si system. However, these results can be qualitatively understood. The binary Nb–Si system contains a number of highly stable silicides, which indicates a strong interaction between the two elements. Table 2 presents the results of chemical analyses (EDX and WDX) of the Laves phase and the ferrite matrix for two of the alloys studied. For the 1% Nb + 0.25% Si alloy the Laves phase was found to contain 40 wt.% Nb while the Nb content of the ferrite matrix was below the detection limit of EDX. Similarly, the Laves phase contained 2.5 wt.% Si and the Si content in the matrix was below the detection limit. The detection limits for EDX was about 0.5% and for WDX about 0.1%. Using the WDX method in case of the 2% W + 0.5% Nb + 0.25% Si alloy was necessary because of overlapping of the tungsten and silicon lines which limit the application of EDX for quantitative analysis in that case. The results show that the Si and Nb were almost completely incorporated in the Laves phase and have left the matrix devoid of these two elements so that they are not available for diffusion to the external scale.

Fig. 9 shows higher magnification SEM cross-sections of four of the alloys. Internal Ti oxides are evident in all of the images. The alloys 1% Nb + 0.25% Si and 2% W + 1% Nb + 0.25% Si formed only a small number of silica particles at the chromia/alloy interface (see Fig. 9b and d) which is consistent with the low Si content in the ferrite matrix. The 1% Nb + 0.42% Si alloy showed more extensive silica formation at the interface while the 2% W + 1% Nb + 0.25% Si showed a silica distribution similar to the 1% Nb + 0.25% Si alloy. In some areas of Fig. 9b–d, there is undissolved Laves phase in contact with the scale, indicating the thermodynamic stability of this compound.

Fig. 10 presents cross-sections of the reference alloy and the 2% W + 1% Nb + 0.25% Si alloy after 10,000 h oxidation at 800 °C. Both alloys have maintained a protective chromia scale, which is more uniform on the 2% W + 0.5% Nb + 0.25% Si alloy.

3.3. Electrical conductivity of the formed oxide scales

Fig. 11 shows the area specific resistance (ASR) values obtained for the modified steels along with the band of values typically observed for JS-3 or Crofer 22 APU pre-oxidised for 100 h in air at 800 °C. The experimental alloys lie within the range of values measured on 18 samples of JS-3 type alloys. The ASRs were converted into conductivity values, taking into account the metallographically measured oxide thicknesses. Strictly speaking, the surface scales formed on the various materials cannot be characterised using such a conductivity value, because the scales do not consist of a single oxide phase and they grow in an oxygen partial pressure gradient. The estimated value is therefore termed "apparent conductivity". Fig. 12 shows the temperature dependence of the apparent electrical conductivity of the oxide scales for the 2% W + 0.5% Nb + 0.25% Si alloy compared with JS-3 and literature data for a pure chromia forming Cr-ODS alloy [11] and the commercial ferritic 16% CR steel 1.4016-3C [27]. The apparent conductivities for the scales on the other modified steels were similar to that of the 2% W + 0.5% Nb + 0.25% Si alloy but are not presented in Fig. 12 for clarity. The results clearly show higher conductivities for the oxides on the investigated variants than for those on the Cr-ODS alloy.

As can be seen in Fig. 11 the addition of 1% Nb or 2.7% W did not seem to affect substantially the scales electrical resistance. On the other hand silicon additions can be detrimental for the

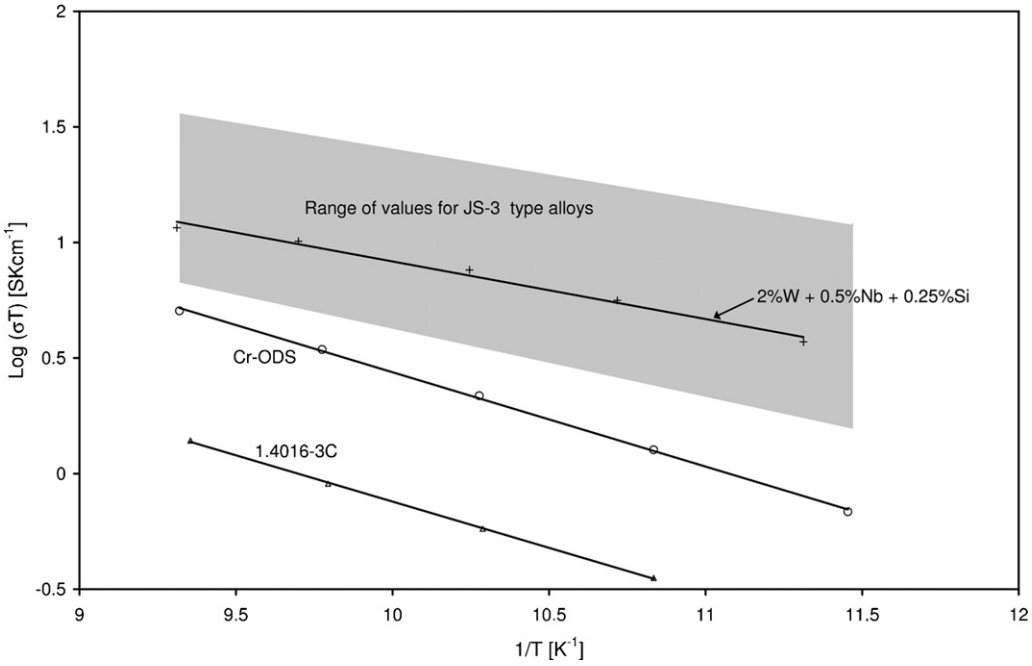

Fig. 12. Apparent conductivity as a function of reciprocal temperature in air for JS-3 and 2% W + 0.5% Nb + 0.25% Si. Data for a Cr-ODS alloy and a commercial 16% Cr ferritic steel (1.4016) were taken from Refs. [11] and [27], respectively.

scale conductivity, as shown for Alloy 446 which contains about 0.29% Si [27]. In the present study an addition of 0.25% Si to the Nb-containing steels seemed to have no detrimental effect on the scale conductivity. This is the result of incorporation of silicon into the Laves phase thereby preventing the formation of a silica sublayer beneath the external surface scale. The range of conductivity data for the oxide scale of the reference alloy relates to measurements on 18 specimens of different batches of JS-3 type alloy. The variation in conductivity values might be associated with changes in the oxide scale morphology caused by reaction with the platinum contact paste. According to the literature, platinum cannot be considered as a completely inert material in contact with the oxide scales formed during long-term testing [7,16]. Fig. 13 shows cross-sections of oxide scales

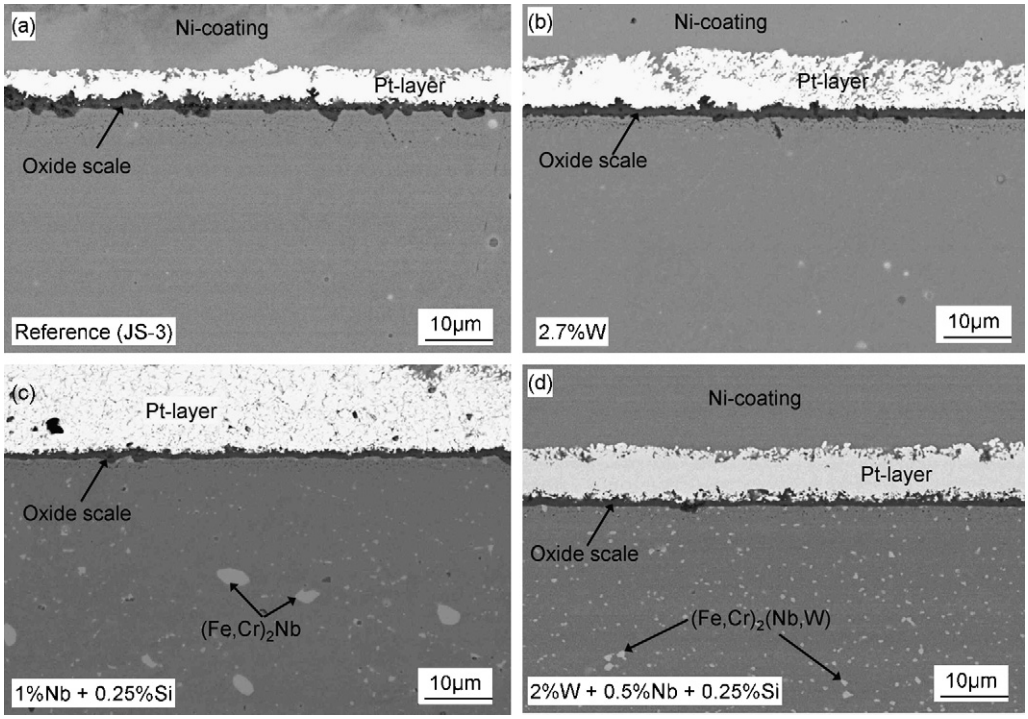

Fig. 13. SEM/BSE images showing microstructures of the oxide scales after conductivity tests: (a) JS-3, (b) 2.7% W, (c) 1% Nb + 0.25% Si, and (d) 2% W + 0.5% Nb + 0.25% Si.

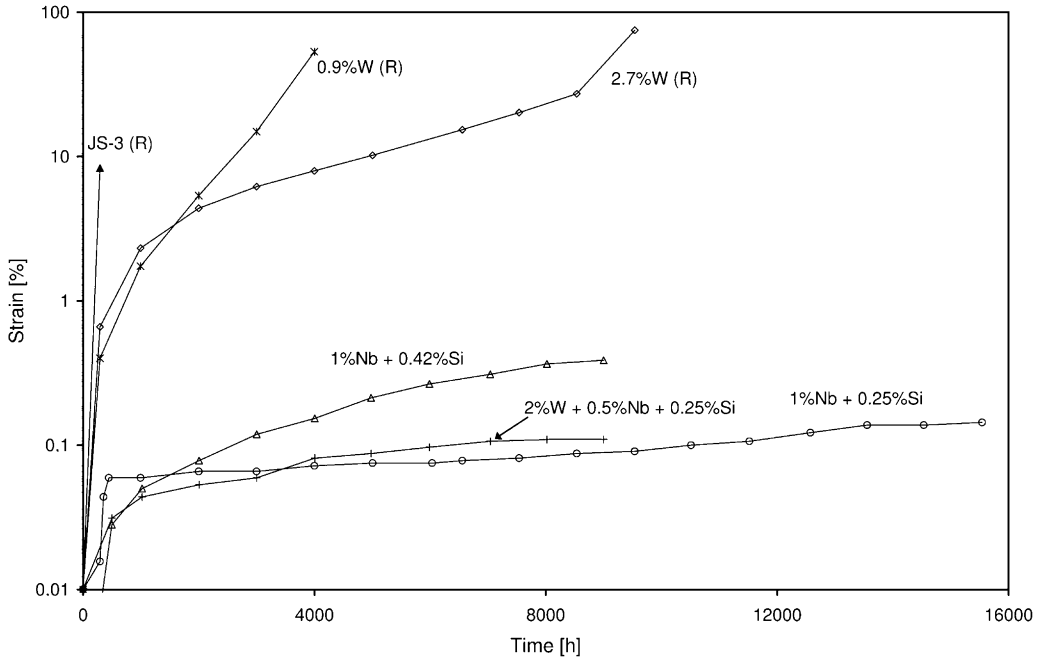

Fig. 14. Strain vs. time for selected steels during creep test at 700 °C and a stress of 10 MPa. R indicates rupture.

on the specimens after the conductivity test. The SEM images show that the oxide scale morphology on JS-3 differed slightly from that on the W/Nb/Si-containing variant. The oxide scale on the JS-3 showed an irregular thickness caused by reaction of oxide scale constituents with platinum and protrusions of the new oxide formed inside the metal matrix, in agreement with observations in Ref. [16]. The oxide scales formed on the new variants were more regular and seemed to be more resistant to "platinum attack".

3.4. Creep tests

Fig. 14 shows creep strain versus time curves for selected steels at 700 °C and a stress of 10 MPa. JS-3 subjected to a stress of 10 MPa at 700 °C exhibited rupture after only 447 h with 8.3% creep strain. The addition of 2.7% tungsten significantly increased the creep strength. In the present study, the tungsten alloyed steel exhibited rupture after 9698 h with 76% creep strain. This result in combination with the results of microstruc-

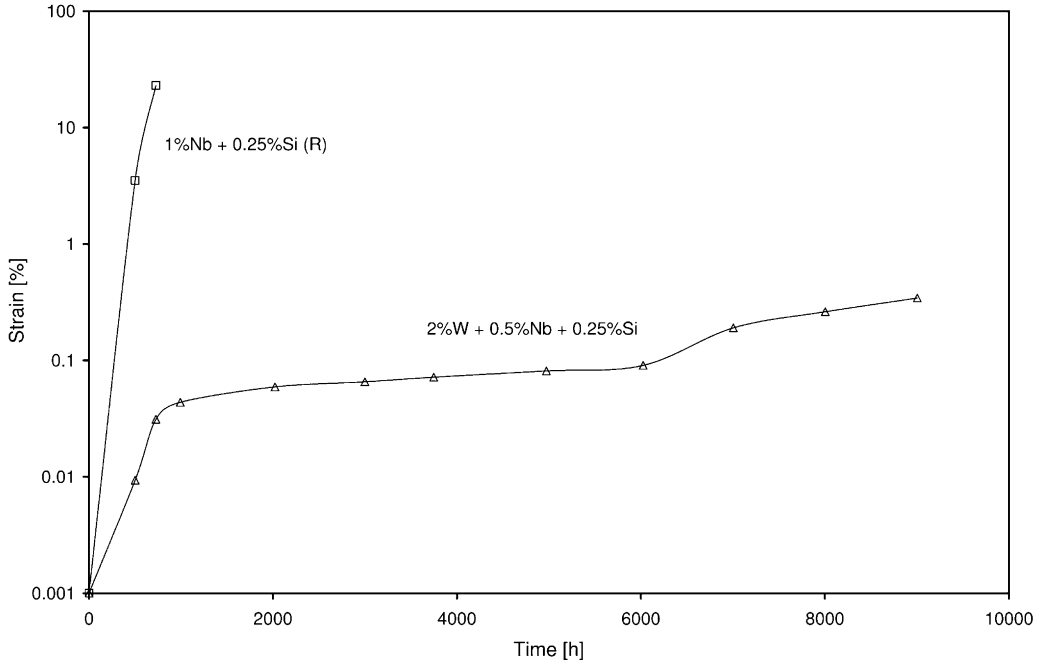

Fig. 15. Strain vs. time for selected steels during creep test at 800 °C and a stress of 10 MPa. R indicates rupture.

tural investigations clearly shows that solid solution strengthening of ferrite with tungsten can significantly increase the creep strength of the ferritic steel. Further improvement of the creep properties can be obtained by additional precipitation strengthening with Laves phase. The steel with 1% Nb and 0.25% Si exhibited 0.09% creep strain after 9539 h under the same conditions. Combined additions of W, Nb and Si gave similar results to the alloys modified only with Nb and Si at 700 °C but were even more effective at higher temperatures resulting in a remarkable improvement in creep strength even at 800 °C (Fig. 15).

Comparison of creep curves for the 2% W + 0.5% Nb + 0.25% Si alloy at 700 and 800 °C (Figs. 14 and 15) show that at both temperatures the alloy exhibited nearly the same creep strain of about 0.07% after 6000 h.

Addition of the alloying elements W/Nb/Si will not only affect the high-temperature creep resistance but also the tensile properties including a possible deterioration of ductility and workability. Tensile tests conducted on the steel alloyed with 2% W–0.5% Nb–0.25% Si at room temperature showed that the tensile strength was nearly the same as that of JS-3. Tensile tests conducted at 700 and 800 °C showed an approximately 60% increase in tensile strength compared with JS-3. Although the fracture elongation in comparison with JS-3 was reduced from about 38 to 23% at room temperature and from about 54 to 25% at 700 °C, it is expected that this will not significantly affect the ability to fabricate suitable semi-finished products.

4. Summary and conclusions

Using optimised, combined additions of Nb, W and Si the creep strength of high-Cr ferritic steels can be substantially increased. The addition of minor amounts of Si largely supresses the adverse effect of Nb on the oxidation behaviour, resulting in slowly growing, well-adhering surface oxide scales, which possess a high electronic conductivity at SOFC operation temperatures. Of special importance for the cold workability of the improved steel is the relatively high room temperature fracture elongation of approximately 23%. Thus, the combined additions of Nb and W, along with Si, resulted in an alloy with a substantially higher creep strength than JS-3 without deteriorating the oxidation resistance and the electrical conductivity of the oxide scales.

References

[1] J. Piron-Abellan, F. Tietz, V. Shemet, A. Gil, T. Ladwein, L. Singheiser, W.J. Quadakkers, in: J. Huijsmans (Ed.), Proceedings of the 5th European Solid Oxide Fuel Cell Forum, European Fuel Cell Group, Lucerne, Switzerland, 2002, p. 248.
[2] R. Hojda, W. Heimann, W.J. Quadakkers, ThyssenKrupp Techforum (2003) 20–23.
[3] W.J. Quadakkers, J. Piron-Abellan, V. Shemet, L. Singheiser, Mater. High Temp. 20 (2003) 115–127.
[4] K. Honegger, A. Plas, R. Diethelm, W. Glatz, in: H. Yokokawa, S.C. Singhal (Eds.), Proceedings of the SOFC-VII, vol. 16, Electrochem. Soc., Pennington, NJ, 2001, p. 803.
[5] T. Uehara, T. Ohno, A. Toji, in: J. Huijsmans (Ed.), Proceedings of the 5th European Solid Oxide Fuel Cell Forum, European Fuel Cell Group, Lucerne, Switzerland, 2002, p. 281.
[6] J.W. Fergus, Mater. Sci. Eng. A 397 (2005) 271–283.
[7] K. Huang, P. Hou, J. Goodenough, Solid State Ionics 129 (2000) 237–250.
[8] T. Horita, Y. Xiong, H. Kishimoto, K. Yamaji, N. Sakai, H. Yokokawa, J. Power Sources 131 (2004) 293–298.
[9] Z. Yang, M. Walker, P. Singh, J.W. Stevenson, T. Norby, J. Electrochem. Soc. 151 (2004) 669–678.
[10] P. Lamp, J. Tachtler, O. Finkenwirth, S. Mukerjee, S. Shaffer, Fuel Cells 3 (2003) 1–7.
[11] P. Huczkowski, N. Christiansen, V. Shemet, L. Niewolak, J. Piron-Abellan, L. Singheiser, W.J. Quadakkers, Fuel Cells 6 (2006) 93–99.
[12] P. Huczkowski, N. Christiansen, V. Shemet, J. Piron-Abellan, L. Singheiser, W.J. Quadakkers, Mater. Corros. 55 (11) (2004) 825–830.
[13] P. Huczkowski, N. Christiansen, V. Shemet, J. Piron-Abellan, L. Singheiser, W.J. Quadakkers, J. Fuel Cell Sci. Technol. 1 (2004) 30–34.
[14] Z. Yang, J. Hardy, M. Walker, G. Xia, S. Simner, J.W. Stevenson, J. Electrochem. Soc. 151 (2004) 1825–1831.
[15] J.E. Hammer, S.J. Laney, R.W. Jackson, K. Coyne, F.S. Pettit, G.H. Meier, Oxid. Met. 67 (2007) 1–38.
[16] P. Huczkowski, W.J. Quadakkers, Effect of geometry and composition of Cr steels on oxide sale properties relevant for interconnector applications in Solid Oxide Fuel Cells (SOFCs), Report Forschungszentrums Jülich, Energy Technology 65, 2007, ISBN 978-3-89336-484-8.
[17] S.J. Laney, Modifying ferritic stainless steels for solid oxide fuel cell applications, Ph.D. Thesis, University of Pittsburgh, USA, 2007.
[18] A. Holt, P. Kofstad, Solid State Ionics 117 (1999) 21–25.
[19] P.J. Ennis, W.J. S Quadakkers, Proceedings of the Conference of High Temperature Alloys—Their Exploitable Potential, October 15–17, 1985, Petten, NL, Elsevier, London, 1988, pp. 465–474.
[20] F.J. Piron Abellan, W.J. Quadakkers, Development of ferritic steels for application as interconnect materials for intermediate temperature solid oxide fuel cells (SOFCs) Report, Forschungszentrum Jülich, Jülich, Germany, Jül-4710, ISSN 0944-2952, 2005.
[21] K. Yamamoto, Y. Kimura, F.G. Wei, Y. Mishima, Mater. Sci. Eng. 329 (2002) 249–254.
[22] P.J. Ennis, in: R. Viswanathan (Ed.), Proceedings of the 3rd EPRI Conference on Advances in Materials Technology for Fossil Power Plants, Swansea, UK, 2001, p. 187.
[23] J. Mougin, M. Dupeux, L. Antoni, A. Galerie, Mater. Sci. Eng. 359 (2003) 44–51.
[24] N. Fujita, K. Ohmura, A. Yamamoto, Mater. Sci. Eng. 351 (2003) 272–281.
[25] Y. Wouters, G. Bamba, A. Galerie, M. Mermoux, J.P. Petit, Mater. Sci. Forum 461–464 (2004) 839–846.
[26] L. Mikkelsen, S. Linderoth, J.B. Bilde-Sorenson, Mater. Sci. Forum 461–464 (2004) 117–122.
[27] W.J. Quadakkers, J. Piron-Abellan, V. Shemet, Mater. Res. 7 (2004) 1–6.